Ndao et al. EURASIP Journal on Wireless Communications and Networking 2013, 2013:167
http://jwcn.eurasipjournals.com/content/2013/1/167

EURASIP Journal on Wireless Communications and Networking
a SpringerOpen Journal

RESEARCH Open Access

Development and test of a trans-horizon communication system based on a MIMO architecture

Papa Moussa Ndao[1], Yvon Erhel[2*], Dominique Lemur[1], Martial Oger[1] and Jérôme Le Masson[2]

Abstract

A multiple-input multiple-output (MIMO) system for trans-horizon radio communications within the high-frequency (HF) band (3 to 30 MHz) is presented. The diversity of transmitted polarizations is proposed as an alternative to spatial diversity in order to limit the aperture of antenna arrays at both ends of the radio link. In a theoretical step providing the estimation of capacity gain for different MIMO architectures, a 2 × 2 MIMO solution transmitting two complementary circular polarizations is identified as a balanced trade-off between performance increase and complexity. The design of the corresponding system is described with a focus on antenna arrays and the kind of signal processing that should be implemented. This novel communication system has been tested on a 280-km-long radio link. The first results underline a data transfer rate reaching a value of 24.09 kbps (in a 4.2-kHz bandwidth) that significantly exceeds the current standards for HF modems.

Keywords: Ionosphere, MIMO, Polarization diversity, Compact array, Capacity gain

Introduction

High-frequency (HF) radiowaves (carrier frequency in the 3-to-30-MHz interval), when propagated through the ionosphere, can achieve long haul transmissions with a minimal infrastructure when compared to satellite links. However, this specific channel presents a reduced coherence bandwidth estimated in most cases to several kilohertz. Consequently, the performances of current equipment in terms of data transfer rate appear moderate. For example, the military STANAG 5066/G standard indicates data rates up to 9.6 kbps in a 3-kHz bandwidth, and the digital radio mondiale broadcasting standard specifies a maximum value of 18 kbits/s in a 10-kHz bandwidth.

Aiming at a significant increase in channel capacity, this work addresses the design of a multiple-input multiple-output (MIMO) architecture for trans-horizon communications. MIMO solutions were quite successful in the conception of recent wireless systems in UHF-EHF bands such as indoor networks (WLAN). However, no transposition in the HF band is yet to be worked out due to the conjunction of two limiting factors for the set up of efficient antenna arrays with spatial diversity: decametric wavelengths and reduced angular separation of radio waves emerging from the ionosphere. Indeed, classical results generally recommend an inter element spacing of several wavelengths [1], a parameter equal up to 100 m in this frequency band. Moreover, the small dispersion in elevation and azimuth angles for incident waves at the receive site requires an additional spacing increase to reduce the channel correlation. Finally, the implementation of a standard MIMO solution at HF appears unrealistic for a reason of available space [2,3] and prohibitive wire lengths.

Therefore, this paper proposes an alternative based on the diversity of the transmitted polarizations. This original idea relies on the existence of two propagation modes through the ionosphere resulting from the medium anisotropy; these two solutions for the propagation equations are characterized by two different sets of parameters such as attenuation or group delay: the corresponding channel impulse responses present a low level of correlation which is suitable for efficient MIMO transmission.

* Correspondence: yvon.erhel@st-cyr.terre-net.defense.gouv.fr
[2]French Military Academy Saint-Cyr Coetquidan, Guer 56381, France
Full list of author information is available at the end of the article

By means of a model of ionosphere associated with a ray tracing software, theoretical capacities for different HF MIMO channels are then estimated. A suboptimal solution consisting in the transmission of two complementary circular polarizations appears as a balanced trade off between capacity gain and complexity.

According to these conclusions, an entire 2 × 2 HF-MIMO system has been developed with compact antenna arrays at both ends and standard solutions for signal processing: transmission of data blocks, frequency domain equalization, and periodically refreshed channel estimation using training sequences.

Experiments have been carried out on a 280-km-long radio link. A preliminary step of non-modulated carrier transmission aimed at checking the effective generation of circular polarizations with the antennas selected for the project. Then, the concept of diversely polarized HF-MIMO architecture has been validated through the estimation of channel transfer functions with a relatively low level of correlation. The data transfer rate (in a spatial multiplexing scheme) reached up to 24.2 kbps (in a 4.2-kHz bandwidth), with a good quality of service and a spectral efficiency significantly exceeding the values encountered in current standards.

This article is organized as follows: section 'Elements of EM propagation in the ionosphere' gives a brief review of physics in the ionosphere, focusing on the existence of two propagation modes; section 'Ionospheric channel simulation' describes the different modules involved in a realistic simulation of ionospheric propagation; after the introduction of the polarization diversity concept, section 'Capacity of a HF-MIMO system with polarization diversity' focuses on the estimation of theoretical channel capacity for different HF-MIMO channels and exhibits the selected solution; section 'Design of the MIMO system' describes the different parts of the communication system and the signal-processing techniques which are implemented in the receivers; finally, section 'Experimental validation' presents the most significant results of experiments which have been carried out to validate the proposed concept, and a conclusion highlights the system performances.

Elements of EM propagation in the ionosphere

Existence of two propagation modes

The solar activity is responsible for the ionization of chemical constituents in the upper atmosphere extending from about 60 km to more than 1,000 km above ground level. This physical phenomenon is locally quantified by the electron density N, considered as a function of altitude. Considering its variations, the ionosphere appears as a non-homogeneous plasma with several so-called layers defined as regions that are confined between two local minimums of the electron density. This medium is also anisotropic since the direction of the terrestrial geomagnetic field has a particular role when resolving Maxwell's equations. Consequently, the solution proposed by Appleton and Hartree [1,4], in the context of the so-called magneto-ionic theory, underlines the existence of two propagation modes named ordinary (denoted O) and extraordinary (denoted X). As the corresponding refractive indices n_O and n_X continuously varies with altitude, the wave refraction is observed and permits over-the-horizon transmissions. Simplified expressions for n_O and n_X at point M in the ionosphere are given by Equation 1 in which sign + is associated with n_O and sign – with n_X.

$$n_{O,X}^2(M) = 1 - \frac{2X(1-X)}{2(1-X) - Y_T^2 \pm \sqrt{Y_T^4 + 4(1-X)^2 Y_L^2}}, \quad (1)$$

$$\text{with } X = N(M).e^2/4\pi^2\varepsilon_o m f^2,$$

where $N(M)$ is the electron density at point M, e is the elementary electronic charge, m is the electron mass, ε_o is the vacuum permittivity, and f is the frequency of the electromagnetic wave,

$$\text{with } Y_L = \frac{eB_o(M)}{2\pi m f} cos\theta,$$

where $B_o(M)$ is the modulus of the local terrestrial magnetic field and θ is the angle between this vector and the propagation direction,

$$\text{and } Y_T = \frac{eB_o(M)}{2\pi m f} sin\theta.$$

Elliptical polarization

In addition, the magneto-ionic theory [1,4] describes the polarization for O and X modes propagating in the ionospheric plasma and gives tools to predict its significant parameters in a deterministic approach. The electric field, for example, is in most cases elliptically polarized but non-transverse. However, it becomes transverse electromagnetic (TEM)-polarized at the lower bounds of the ionosphere according to the conditions of Budden [5] which express that the electron density $N(M)$ tends towards zero (and jointly the longitudinal component of the electric field) at these positions. Thus, a radio wave emerging from the ionosphere with a given TEM elliptical polarization keeps its characteristics unchanged along its propagation to the receiving site.

The elliptical shape of polarization is entirely described with two parameters. The first one is the polarization

ratio (real) η: its absolute value quantifies the respective lengths of the two axes of the ellipse along which the electrical field rotates; its sign indicates the clockwise (+) or counterclockwise (–) rotation. The second parameter is the inclination angle α evaluated in the plane of the wave front between the ellipse main axis and the local horizontal. The expressions of η and α have been first derived by Appleton [4] and, among other parameters, depend on the angle θ between the propagation vector and the terrestrial magnetic field.

The two limiting polarizations at the entry and exit of the ionosphere are defined as the local *O* or *X* polarizations [5]. For a direction of propagation at the entry identified by azimuth and elevation angles $\delta_{en} = [Az_{en}, El_{en}]$, the deterministic computation of polarization parameters η_{enO}, η_{enX}, α_{enO} and α_{enX} is possible by reference to a database describing the terrestrial geomagnetic field. The same method provides the corresponding values η_{exO}, η_{exX}, α_{exO} and α_{exX} at the exit point for a radio wave emerging towards the receiving site in a direction characterized by angles $\delta_{ex} = [Az_{ex}, El_{ex}]$.

Moreover, polarization ratios for a couple of complementary modes verify the constraint of orthogonality [6]:

$$\eta_{enO} \cdot \eta_{enX} = \eta_{exO} \cdot \eta_{exX} = -1 \quad (2)$$

As a consequence, any polarization of a TEM wave can be expressed as a linear combination of these two modes.

Ionospheric channel simulation

Simulations of an ionospheric radio link combine a model of the electron density, considered for simplification as a function of the altitude only (assuming the absence of horizontal gradients), and a ray tracing software.

A current model for electron density, called multi-quasi-parabolic (MQP) profile, considers its variations as a succession of parabolic portions [7]. Despite possible continuity defaults when deriving the corresponding refractive index, this representation is known as effective. Each layer (represented by a portion of the profile) is characterized by the three parameters: local maximum electron density (or maximum plasma frequency), corresponding height, and semi-thickness. Their typical values and long term (month or year scale) or short term (day and hour in a day) variations are predicted by ionospheric forecast software like LOCAPI [8]. Alternatively, these parameters may be estimated from radio sounding data covering the geographic area of the radio link.

The second step in the channel simulation consists in programming a ray tracing method: for a given point-to-point radio link and a fixed carrier frequency *fo*, rays are launched in any elevation in the 0° to 90° interval and an azimuth defined by the great circle joining transmitter and receiver [6]. The paths of interest are identified as emerging at a given maximal distance of the receiving site. Such a simple classical isotropic approach for ray tracing as the Snell-Descartes law is not suitable at this stage due to the particular role of the terrestrial magnetic field. A general and elegant numerical solution deriving six first-order differential equations based on Hamiltonian optics is implemented in a solution proposed by Jones [9]. This versatile software allows the introduction of different density profiles (such as the MQP model selected in this work) and the addition of ionospheric perturbations like gravity waves that generate displacements in the ionized layers and affect the carrier frequency with a Doppler shift.

For each propagation mode *O* and *X*, the computation outputs are attenuation, group delay, angles of arrival, and optionally, Doppler frequency shift. Additionally, the geographical coordinates of the ionosphere entry and exit points are estimated; then, the local data relative to the terrestrial geomagnetic field, in association with the identified directions of propagation, are extracted to compute the corresponding parameters of the limiting polarizations. For further exploitation, path attenuations and group delays are combined in an estimation of the channel complex transfer functions $H_{cO}(fo)$ and $H_{cX}(fo)$ relative to each mode.

As an illustration, Table 1 gives the computation outputs for an example of radio link. The scenario involves transmission over a ground distance of 900 km operating with a non-modulated carrier frequency equal to 7.5 MHz. The transmitting site has these coordinates: latitude 48°N, and longitude 2°W. The radio link is oriented in azimuth 170°. The date corresponds to a minimum in solar activity, which induces poor conditions for the propagation and consequently strong attenuations. The ray tracing program indicates a propagation scheme with four paths and the existence of limiting polarizations which are quasi-circular and, in this particular case, the modulus of polarization ratios being close to one. For each path, the columns of Table 1 provides the values of elevation of transmitted and received rays, polarization ratios at the entry and exit points, group delay, and attenuation. If a wideband characterization is requested, the computation of $H_{cO}(fo)$ and $H_{cX}(fo)$ is repeated for different values of the carrier frequency fo in an interval which largely exceeds the coherence bandwidth of the ionospheric channel considered as frequency selective.

Capacity of a HF-MIMO system with polarization diversity

Benefit of polarization diversity

As mentioned in the introduction, the implementation of a classical MIMO architecture for applications in the HF band must cope with a problem of available space.

Table 1 Parameters of the four-path propagation

Elevation (degrees)	Polarization ratio η_{en} (entry point)	Polarization ratio η_{ex} (exit point)	Group delay (ms)	Attenuation (dB)	Mode
11.38	+1.03	+1.01	3.08	102.4	*X*
11.48	−0.97	−0.99	3.09	102.4	*O*
25.01	−0.94	−0.95	3.32	103.6	*O*
24.57	+1.06	+1.05	3.33	103.7	*X*

Indeed, the reduced angular separation of transmitted rays requires an inter antenna spacing which largely exceeds the equivalent of several wavelengths, the latter having decametric values in the present context. Consequently, the size of antenna arrays would appear prohibitive in a setup based on spatial diversity only [10]. Therefore, there is a need for an alternative solution using relatively compact arrays at both ends of the radio link. The original idea of this work refers to the existence of two propagation modes *O* and *X* in the ionosphere. Assuming that one limiting polarization (*O* or *X*) is excited at the ionosphere entry thanks to an ad hoc transmitting antenna, the only corresponding propagation mode is observed in the channel and emerges with predictable values of parameters η and α. In a point-to-point transmission, the channel transfer functions $H_{cO}(f)$ and $H_{cX}(f)$ relative to the two modes present a low level of correlation due to the differences affecting the propagation parameters (attenuations, group delays,...) associated to each mode. Even in the absence of spatial diversity, the generation of different transmitted polarizations induces a reduction of channel correlation which is suitable for the implementation of MIMO techniques.

The ideal configuration to optimize the capacity gain would be to generate at the transmit end the two limiting polarizations predicted at the ionosphere entry point: in this case, the ionized medium would act like two nearly independent sub-channels. This solution comes up against the difficulty to design antennas exciting an elliptical polarization with constrained parameters η and α, the values of which are subject to temporal variations (hour in day, day in year,...), making the realization quite hazardous. For the following, realistic solutions consider the generation of standard polarizations: orthogonal linear or complementary circular polarizations.

Computation of MIMO channel capacity

This section presents the successive steps in the estimation of channel capacity for MIMO radio links with polarization diversity. Resorting to the deterministic modelization of the ionosphere (considered as a frequency-selective channel) described above, it is based on the calculation of the channel transfer function for any configuration of the transmitted polarization and receive antenna.

At first, we must note that the estimations of $H_{cO}(f)$ and $H_{cX}(f)$ assume the use of isotropic sensors. Relatively to a given receiver setup, they are complemented in the effective transfer functions $H_O(f)$ and $H_X(f)$ that take the receiver antenna gains into account. These gains are calculated by combining the characteristics of the polarization emerging from the ionosphere, the angles of arrival and the antenna geometry.

In a second step, a given configuration of transmitted polarization denoted *P* (for example, vertical linear) is decomposed as a linear combination of polarizations *O* and *X* with tap coefficients denoted λ_{PO} and λ_{PX}. The effective channel transfer function for that transmitted polarization (containing the receive antenna gain) is then expressed as:

$$\mathrm{H_P(f)} = \lambda_{\mathrm{PO}}\mathrm{H_O(f)} + \lambda_{\mathrm{PX}}\mathrm{H_X(f)}. \tag{3}$$

In the MIMO architecture with polarization diversity that is proposed for the project, *N* transmit antennas generate different polarizations, their spacing being small if compared with the wavelength so that they appear collocated. The index $i = 1,...,N$ identifying one transmitted polarization P_i, the couple of tap coefficients in the decomposition in the *O*-*X* basis is denoted $(\lambda_{iO}, \lambda_{iX})$.

At the receive end, the antenna setup involves *M* different and collocated sensors: the diversity results from the difference in antenna gains relatively to one incident wave, each sensor presenting its specific sensibility to the received polarization. Consequently, the effective channel transfer functions (including the receive antenna gain) must be distinguished regarding the sensor of interest. If $j = 1,...,M$ is the index identifying a receive antenna, the effective channel function for a transmitted polarization P_i and a sensor *j* is expressed as:

$$\mathrm{H_{ji}(f)} = \lambda_{\mathrm{iO}}\mathrm{H_{jO}(f)} + \lambda_{\mathrm{iX}}\mathrm{H_{jX}(f)}, \tag{4}$$

where $H_{jO}(f)$ and $H_{jX}(f)$ are the effective transfer functions for *O* and *X* modes, including the gain of sensor *j*.

For each frequency bin f_n in the spectral band of interest, the MIMO channel matrix is then expressed as:

$$\mathbf{H}(\mathrm{f_n}) = \begin{bmatrix} \mathrm{H_{11}(f_n)} & \mathrm{H_{21}(f_n)} & .... & \mathrm{H_{1n}(f_n)} \\ \mathrm{H_{21}(f_n)} & \mathrm{H_{22}(f_n)} & ... & \mathrm{H_{2n}(f_n)} \\ .... & ... & ... & ... \\ \mathrm{H_{M1}(f_n)} & \mathrm{H_{M2}(f_n)} & ... & \mathrm{H_{MN}(f_n)} \end{bmatrix} \tag{5}$$

Finally, the theoretical capacity of the N × M MIMO system with polarization diversity (frequency selective

and deterministic channel unknown at the transmitter) is calculated with reference to the channel matrix estimated for N_f frequency bins in the considered bandwidth [11]:

$$C_{FS} = \frac{1}{N_f}\sum_{n=1}^{N_f}\log_2\left[\det\left(\mathbf{I}+\frac{SNR}{N}\mathbf{H}(f_n)\mathbf{H}(f_n)^H\right)\right], \quad (6)$$

where $\mathbf{I}$ is the identity matrix of rank M and SNR is the signal-to-noise ratio.

Comparison of different MIMO solutions with polarization diversity

In this paragraph, different configurations of transmitted polarizations are considered and the corresponding channel capacities are estimated and compared in two scenarios of propagation. The main differences in these two schemes lie in the characteristics of the limiting polarizations at the entry point of the ionosphere: *O* and *X* modes present a standard elliptical polarization in scenario #1 and a quasi-circular polarization in scenario #2 as indicated in Table 2, exhibiting parameters (including values of polarization ratio η_{en} at the entry point) predicted by the channel simulation.

For the transmission system, configuration #1 involves two linear orthogonal polarizations, assuming that the directions of vibration are superimposed with the main axis of the two ellipses for *O* and *X* modes. In this theoretical step, the technical solution to satisfy this constraint is not investigated. As an alternative, configuration #2 considers two circular polarizations with opposite senses of rotation.

The capacity estimation requires decomposing each transmitted polarization *P* in the basis of *O* and *X* modes with tap coefficients λ_{PO} and λ_{PX}. As a consequence, the power of a transmit channel splits into two fractions propagating on each mode with a contribution that is proportional to the modulus of the squared tap coefficients. Table 3 indicates the power repartitions in different configurations. For each polarization (generated by transmitters TX1 or TX2), the numerical value represents the fraction of the transmitted power assigned to a mode *O* or *X*. For a given transmitter, the sum of two fractions of power is obviously equal to 1 in each configuration.

It appears that power repartitions are dissymmetric for the two couples of polarizations (two linear or two circular) in scenario #1, but this observation is not valid in scenario #2: as indicated in column 5, the propagation of the two linear polarizations involves *O* and *X* modes with comparable power fractions in this case.

At the receive end, two orthogonal and vertical loop antennas are supposed to be set up with the same phase center. The benefit of a device made up of collocated receive HF antennas has been underlined in a previous realization based on a single-input multiple-output (SIMO) architecture [12]: in the absence of spatial diversity, this solution provides partially uncorrelated acquisitions thanks to the different sensor sensitivities relative to the incoming polarizations.

The capacities for different configurations of 2 × 2 MIMO systems with polarization diversity are then computed according to the method described in section 'Computation of MIMO channel capacity' and Equation 6. The results are compared to the performance of a single-input single-output (SISO) radio link on Figures 1 and 2.

The different plots demonstrate the capacity gain provided in general by the MIMO structure. However, it appears on Figure 2 that the two polarization configurations are not equivalent: in scenario #2, the capacity gain relatively to the SISO case reaches 1.84 for a SNR equal to 30 dB in configuration #2 (circular) and only 1.52 in configuration #1 (linear). The lower performance in the latter case is due to a balanced power repartition which induces a joint excitation of *O* and *X* modes to propagate the information from each transmitter. The level of the inter channel correlation is then relatively high since the transfer function of each channel combines the expressions $H_{jO}(f)$ and $H_{jX}(f)$ with tap weights of comparable magnitude.

On the contrary, if two circular polarizations are transmitted, Table 3 indicates a dissymmetric repartition of power on *O* and *X* modes whatever the propagation scenario (see columns 'Configuration #2' for scenarios #1 and #2). Consequently, the channel transfer function for each circular polarization approximately fits one of the two $H_{jO}(f)$ or $H_{jX}(f)$ and the inter channel correlation is reduced. Unlike configuration #1, polarization configuration #2 induces an increase in the MIMO capacity gain (1.84 for SNR = 30 dB) whatever the propagation scenario #1 or #2. Keeping in mind that the maximum

Table 2 Parameters of the two limiting polarizations

Mode type	Scenario #1		Scenario #2	
	Elevation (°)	Polarization ratio η_{en}	Elevation (°)	Polarization ratio η_{en}
O	24.37	−1.54	35.45	−1.07
X	23.59	+0.65	34.47	+0.93

Table 3 Repartition of power on *O* and *X* modes

Transmitted polarizations		Scenario #1		Scenario#2	
		Configuration #1 linear	Configuration #2 circular	Configuration #1 linear	Configuration#2 circular
TX1	Fraction of power (*O* mode)	0.703	0.05	0.57	0.002
	Fraction of power (*X* mode)	0.297	0.95	0.43	0.998
TX2	Fraction of power (*O* mode)	0.297	0.95	0.43	0.998
	Fraction of power (*X* mode)	0.703	0.05	0.57	0.002

capacity gain is equal to 2, in the case of perfectly uncorrelated channels, this estimated value is quite encouraging.

The only situation for which the couple of linear polarizations could appear more effective corresponds to the existence of linear limiting polarizations at the ionosphere entry point. This case presents a low occurrence and, additionally, would demand that the axes of the transmitted fields be superimposed with the directions of the limiting polarizations, the orientation of which varies with time: the technical challenge appears unrealistic to overcome. Only the generation of linear polarizations with fixed field directions seems possible, and as demonstrated on Figures 1 and 2, it is better anyway to consider the excitation of two complementary circular polarizations.

A last investigation involves a 3 × 3 MIMO configuration obtained with the addition of a linear polarization to the couple of circular polarizations at the transmit end and the setup of a horizontal third loop antenna at the receive end. As plotted on Figure 3, the capacity is not improved in this case. This can be explained by the number of propagation modes which are physically limited to 2. An increase in the number of transmit channels generates additional transfer functions which are linear combinations of the only two $H_{jO}(f)$ and $H_{jX}(f)$: the rank of matrix $\mathbf{H}(f_n)\mathbf{H}(f_n)^H$ remains equal to 2. This pessimistic conclusion concerning 3 × 3 MIMO channels should however be mitigated in multi-hop propagation schemes with ground reflections.

As a consequence of these simulations, the next stage of the project only investigates a practical solution with two transmitting channels that appears as a balanced trade-off between capacity gain and complexity: the following section describes the conception of a 2 × 2 MIMO system based on polarization diversity at both transmit and receive ends.

Design of the MIMO system

Though most recent developments in the area of digital communications resort to multi-carrier signals, this project is intentionally based on a single carrier waveform. The reason stands in the high level of mean transmitted power which is requested (order of magnitude equal to

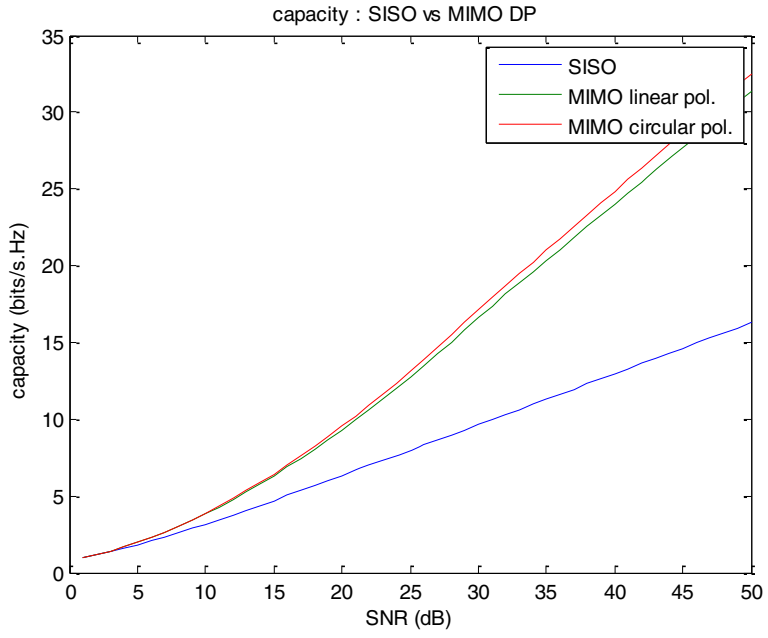

Figure 1 Capacity of a 2 × 2 MIMO channel with polarization diversity; two configurations; scenario #1.

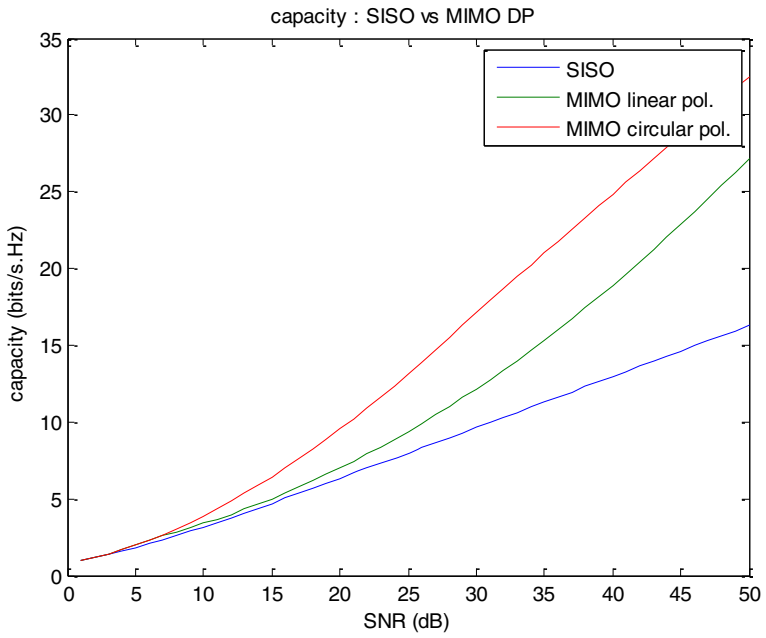

Figure 2 Capacity of a 2 × 2 MIMO channel with polarization diversity; two configurations; scenario #2.

500 W per channel) to achieve radio links over distances exceeding 1,000 km. In a multi-carrier context, the power amplifier linearity requires very costly oversizing, considering that the peak-to-average power ratio (PAPR) of multi-carrier signals is typically close to 6 dB. A limited budget for equipment justifies the choice of a single carrier which nevertheless is compatible with an efficient signal processing in the frequency domain as requested in MIMO architectures. A synopsis of the transmission system is depicted in Figure 4.

Antenna arrays

The generation of two complementary circular polarizations at the transmit end resorts to different solutions. Channel #1 involves a wideband log-spiral antenna, model SPR230, with a 80-m diameter. Its design uses log-

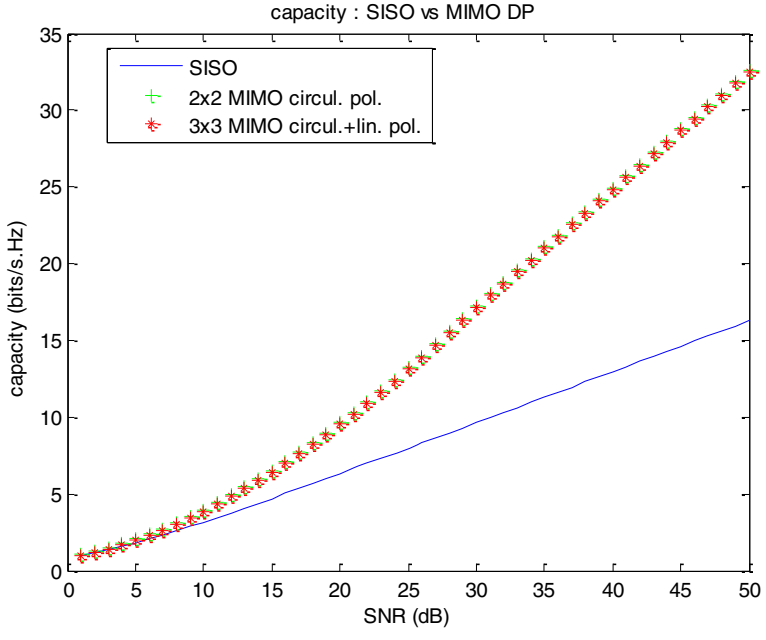

Figure 3 2 × 2 MIMO and 3 × 3 MIMO capacities.

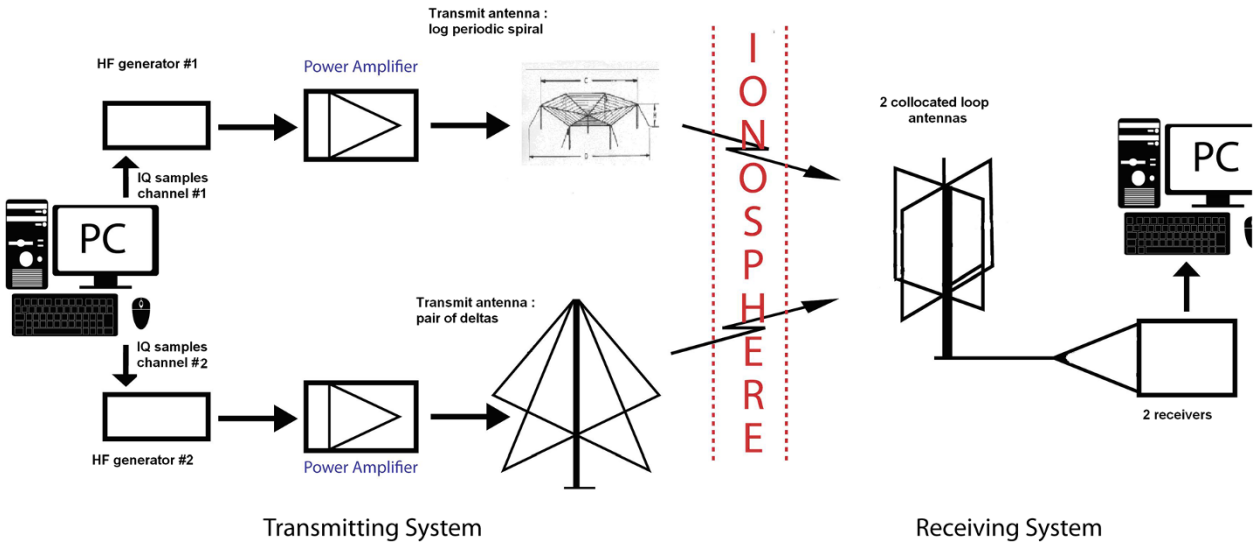

Figure 4 Synopsis of the HF-MIMO system with polarization diversity.

periodic principles to achieve broadband performances while mounted over standard soils. The spiral alumoweld wire curtain provides a right-hand circular polarization with a beam directed to the zenith (for frequencies below 20 MHz). The laboratory having only one antenna of this type, the set up for channel #2 is based on two orthogonal progressive wave delta antennas, each of them being 34-m long and 14-m high, fed with two identical signals presenting a phase shift of $\pi/2$, the sign of which is chosen to generate the opposite sense of rotation if compared to the first channel. The antenna devices are separated by a distance of 150 m and appear as a transmit array with a (relatively) small aperture.

As mentioned in the paragraph describing the computation of MIMO channel capacity, a HF receive antenna has a directional gain that is computed by combining the polarization parameters for the wave emerging from the ionosphere, the direction of arrival and the antenna geometry. This gain appears complex valued as the electromagnetic field rotates on an elliptical trajectory in the plane of wave. It varies with the structure of the incident polarization. In a previous project focused on the conception of a SIMO system [12,13], an original device of two HF active antennas with the same phase center was developed and also selected for the MIMO realization. An optimization in the diversity of their directional responses and in their mutual coupling emphasized the selection of two orthogonal vertical loop antennas set up in a total volume of 2 m^3. The benefit provided by this compact device in the field of array processing is illustrated in Figure 5 plotting synchronous acquisitions on the two channels.

The presence of multiple paths, generated by the ionospheric channel, induces fading. It should be noted that the maximum of power do not appear at the same time on the two channels, indicating a relatively low level of cross correlation despite absence of space diversity. The explanation stands in the diversity of the directional antenna gains which operate as complex valued weighing factors on the incident sources. Each acquisition appears as a sum of several sources with different phase shifts, the distribution of which varies from a channel to another: therefore, the chronograms present significant differences.

Signal processing

The superposition of different transmitted signals in MIMO architectures requires, at the receiving end, a multi-channel equalization operating in the frequency domain (FDE). Since a single carrier waveform has been selected, the equalizer in the receiving system is then characterized as 'single carrier and frequency domain equalization SC-FDE', the principles of which are described in [14].

The signal processing techniques implemented in the demonstrator are conventional. FDE in the receiver uses a fast Fourier transform (FFT) operation to estimate a

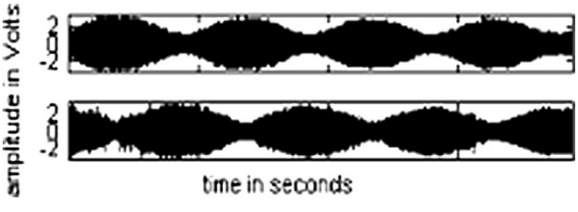

Figure 5 Acquisitions on the two collocated HF antennas.

received spectrum with a collection of M acquisitions called a block. At this stage of the project, the equalization is based on a zero-forcing (ZF) method. The ZF MIMO-FDE [15] is based on the inversion of the channel matrix for each frequency bin (with dimensions 2 × 2 in a 2 × 2 MIMO system). During the transmission, this matrix is estimated by means of Chu training sequences [16] presenting good spectral properties. They are repeated with a period that is adjusted with respect to the channel stationarity duration.

During the effective transmission (data unknown at the receive end), s_{ti}^{k} denotes the transmitted block at instant k on the transmit antenna i; $\tilde{s}ti^{k}(\mathrm{f})$, its FFT transform; s_{rj}^{k}, the received block at instant k on the receive antenna j; and $\tilde{s}_{rj}{}^{k}(\mathrm{f})$, its FFT transform. In a noiseless scheme, the received signals are expressed as the superposition of the channel outputs:

$$\begin{aligned}\tilde{\mathrm{s}}_{\mathrm{r1}}{}^{\mathrm{k}}(\mathrm{f}) &= \mathrm{Hc}_{11}(\mathrm{f}).\tilde{\mathrm{s}}_{\mathrm{t1}}{}^{\mathrm{k}}(\mathrm{f}) + \mathrm{Hc}_{12}(\mathrm{f}).\tilde{\mathrm{s}}_{\mathrm{t2}}{}^{\mathrm{k}}(\mathrm{f})\\ \tilde{\mathrm{s}}_{\mathrm{r2}}{}^{\mathrm{k}}(\mathrm{f}) &= \mathrm{Hc}_{21}(\mathrm{f}).\tilde{\mathrm{s}}_{\mathrm{t1}}{}^{\mathrm{k}}(\mathrm{f}) + \mathrm{Hc}_{22}(\mathrm{f}).\tilde{\mathrm{s}}_{\mathrm{t2}}{}^{\mathrm{k}}(\mathrm{f}).\end{aligned} \tag{7}$$

For each frequency bin, the values of the transmitted spectrum are given by the inversion of a system of two equations in two unknowns. Practically, this computation operates with the estimated channel frequency responses. The two transmitted data blocks are estimated in the frequency domain according to:

$$\begin{pmatrix}\tilde{\mathrm{s}}_{\mathrm{est1}}{}^{\mathrm{k}}(\mathrm{f})\\ \tilde{\mathrm{s}}_{\mathrm{est2}}{}^{\mathrm{k}}(\mathrm{f})\end{pmatrix} = \begin{bmatrix}\mathrm{Hcest}_{11}(\mathrm{f}) & \mathrm{Hcest}_{12}(\mathrm{f})\\ \mathrm{Hcest}_{21}(\mathrm{f}) & \mathrm{Hcest}_{22}(\mathrm{f})\end{bmatrix}^{-1}.\begin{pmatrix}\tilde{\mathrm{s}}_{\mathrm{r1}}{}^{\mathrm{k}}(\mathrm{f})\\ \tilde{\mathrm{s}}_{\mathrm{r2}}{}^{\mathrm{k}}(\mathrm{f})\end{pmatrix}. \tag{8}$$

The data resulting from the frequency domain ZF equalization are then transposed in the time domain thanks to two IFFT operations, the corresponding samples being passed to the decoding process. Moreover, a cyclic prefix is inserted as overhead in each transmitted block to combat contamination by interblock interference resulting from channel delay spread. Additionally, its presence, introducing a partial periodicity in the data stream, is the basis of time detection (or synchronization) for each block start in the received signal.

Experimental validation

The cornerstone of the project consists in the transmission of two messages through decorrelated channels resorting to the generation of two complementary circular polarizations. A preliminary experimental step aimed at checking the nature of the polarizations excited through the antenna set up.

Polarization checking

The goal of these first experiments is to verify that the antenna devices have the possibility to generate simultaneously two circular polarizations rotating in opposite senses. Tests have been carried out on a very short radio link (30 km) with the transmission of non-modulated signals propagating through the ionosphere. In these singular conditions, with a range largely inferior to the typical heights of ionized layers, the elevation of incident waves at the receive end is close to 90°: this scheme corresponds to the so-called near-vertical-incidence skywave (NVIS) conditions.

At the receive end, two vertical loop antennas are set up in orthogonal directions: east to west orientation for the first, and north to south for the second. The corresponding acquisitions, denoted $x_{\mathrm{EW}}(t)$ and $x_{\mathrm{NS}}(t)$ are combined to provide the receiver outputs as:

$$\begin{aligned}\mathrm{x}_1(\mathrm{t}) &= \mathrm{x}_{\mathrm{EW}}(\mathrm{t}) + j\mathrm{x}_{\mathrm{NS}}(\mathrm{t})\\ \mathrm{x}_2(\mathrm{t}) &= \mathrm{x}_{\mathrm{EW}}(\mathrm{t}) - j\mathrm{x}_{\mathrm{NS}}(\mathrm{t})\end{aligned} \tag{9}$$

In NVIS conditions, this combiner with weighing factors equal to $+/-j$ appears as an optimal polarization filter: one circularly polarized incoming wave induces one of the output signals with a modulus doubled if compared to each individual acquisition and the other with a modulus equal to zero, the respective role of $x_1(t)$ and $x_2(t)$ depending on the sense of rotation.

In the experiment, the two transmitting channels generate two carriers with a slight frequency shift equal to 5 Hz in order to identify the different contributions in the combiner outputs. To validate the effective excitation of complementary circular polarizations, dissymmetric peaks are expected in the output spectrums: the reference carrier frequency should appear as a peak in one of them and be absent in the second; reciprocally, the shifted carrier frequency should be absent in the first spectrum and correspond to a significant peak in the second.

At the beginning of the test, the reference carrier frequency is selected according to the ionospheric propagation conditions. An example of combiner output spectrums is plotted on Figure 6 with a linear scale for amplitude. Detected peaks are separated by an interval of 5 Hz corresponding to the carrier frequency shift. Note that the spectral analysis operates with acquisitions transposed on the intermediate frequency IF (equal to 5 kHz) receiver outputs.

As expected, the spectrum peaks for each output are quite dissymmetric, indicating that the transmitted polarizations are quasi-circular. Output #1 alone has a component at frequency 5.000 kHz: this can be interpreted as the generation by transmit channel #1 of a circular polarization that fits combiner #1. However, if output #2 has a major component at frequency 5.005 kHz, a residual peak of output #1 is visible with an amplitude ratio of nearly −10 dB. This observation suggests

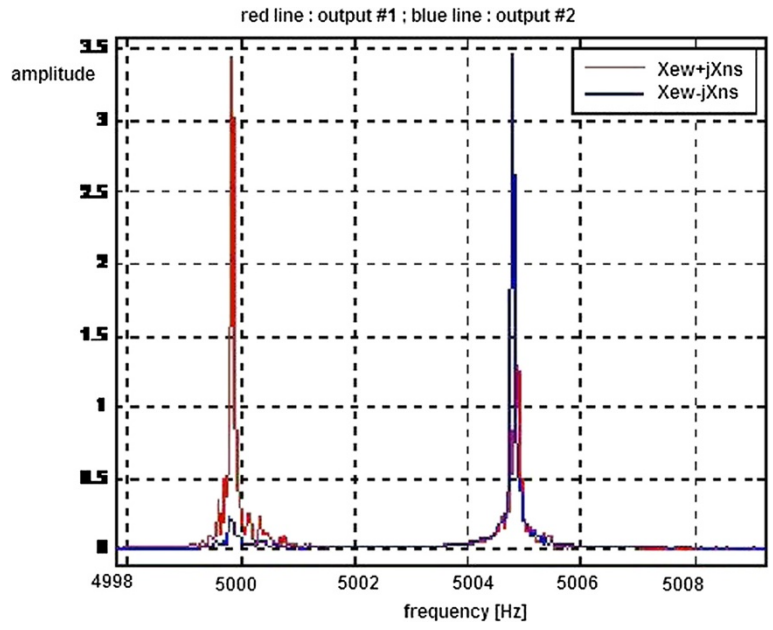

Figure 6 Combiner output spectrums.

that the polarization excited at transmit channel #2 is not perfectly circular. Nevertheless, this small imperfection should not prevent the project from going further.

Data transmission

An experimental 2 × 2 MIMO transmission has been tested between Monterfil (48°20N, 2°03'W) and Lucay (47°13'N, 1°44'E) with a range of 280 km. On 21 April 2011 at 11 h UT, ionograms indicate critical frequencies for the E and F2 layers respectively equal to 3.8 and 7.8 MHz (*O* mode) and 4.7 and 8.5 MHz (*X* mode) as depicted in Figure 7. Consequently, the selected carrier frequency (7.240 MHz) permits propagation of complementary *O* and *X* modes with close reflection heights.

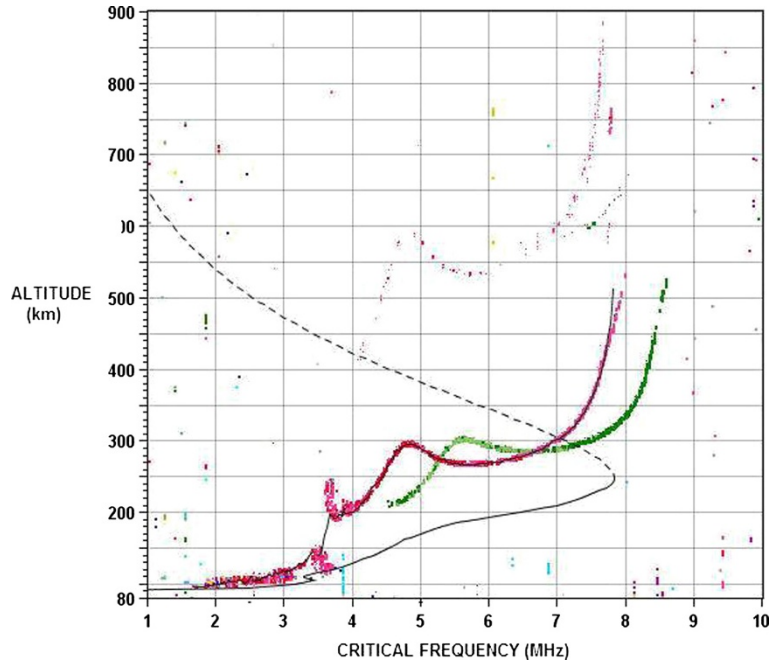

Figure 7 Ionograms; red curve: *O* mode; green curve: *X* mode.

After checking the absence of jammer, a first test involving non-modulated signals has been carried out to adjust each transmitted power (50 W for channel #1 and 200 W for channel #2) in order to observe balanced received levels.

As mentioned in the 'signal processing' paragraph, transmitted messages are organized as a succession of data blocks. The waveform and block parameters have been optimized in a simulation involving both system and channel. Each data block contains 256 complex symbols plus a cyclic prefix of 16 symbols. These symbols belong to a QAM 16 constellation for data transmission and are elements of a Chu sequence for the blocks of channel training. The symbol rate is equal to R = 3,200 bauds. The transmitted spectrum is a classical raised cosine with a roll-off factor equal to 0.3, so that the resulting bandwidth equals 4.2 kHz. In a spatial multiplexing scheme as selected in this test, two independent streams of data are transmitted in a synchronous mode. The effective data transfer rate is then double if compared to the SISO case:

$$D_{\mathrm{MIMO}} = 2 \times 3,200 \times 4 \times \frac{256}{256+16} = 24.09\ kbps.$$

In the data stream, Chu sequences are periodically inserted to refresh the channel estimation. Considering that the stationarity duration of the ionosphere is equal to a few seconds, a new channel estimation, involving two Chu sequences, is processed every sixteen data blocks, i.e., with a period of 1.38 s. Moreover, error measurements are made in the absence of any channel coding: the estimated bit error rates are raw.

Results: channel estimation

The key condition to observe a capacity increase (compared to a SISO solution) is to verify the existence of a partially decorrelated MIMO channel linking transmitters and receivers. The original idea of the project assumes that polarization diversity at the transmitter could be responsible for this reduction of correlation. Therefore, it is quite relevant to compare the four-channel frequency responses (in this 2 × 2 MIMO system) estimated by the means of training sequences. For a given acquisition file, the modulus of the four-channel transfer functions H_{ij}, i = 1,2 and j = 1,2 are plotted on Figure 8 for a frequency interval of 3.2 kHz equal to the symbol rate.

The quasi-periodic shape of some of these plots suggests that, if two complementary modes are effectively excited, a third path is likely present with a differential group delay estimated equal to 1.6 ms. This assumption is confirmed by propagation predictions indicating possible refraction on E and F2 layers.

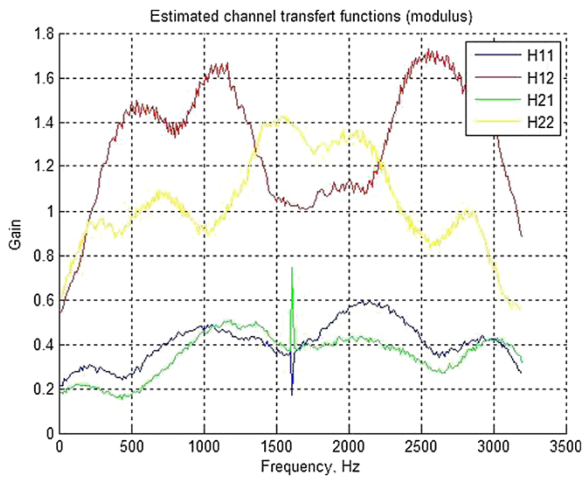

Figure 8 Comparison of the four-transfer functions (modulus).

In addition, Table 4 gives the modulus of inter channel correlation coefficients estimated from samples of the four frequency responses: it indicates a relatively low level of intercorrelation which is suitable for MIMO applications despite reduced spatial diversity at both ends of the radio link. These positive results validate the concept of polarization diversity in this MIMO architecture.

Results: BER measurements

In the spatial multiplexing scheme, the received symbols for each data stream are estimated at the output of the frequency domain equalizers; the corresponding constellations are plotted on Figures 9 and 10. The dispersion of the complex samples around the expected positions appears moderate, which underlines the efficiency of the FDE equalization.

Bit error rate (BER) measurements are carried out on several blocks of 256 complex symbols representing 1,024 binary data. For a given acquisition file and a signal-to-noise ratio equal to 19 dB, the measured BER is equal to 8.0×10^{-3} for channel #1 and 1.2×10^{-2} for channel #2 (raw values without any channel coding). Results indicate a good quality of service and could be improved if necessary with an increase in the transmitted power, the maximum possible value being equal to 500 W per channel with the available equipment.

Table 4 Inter channel correlation coefficients

Correlation	H_{11}	H_{12}	H_{21}	H_{22}
H_{11}	1.0000	0.3822	0.9237	0.7233
H_{12}	0.3822	1.0000	0.4752	0.2414
H_{21}	0.9237	0.4752	1.0000	0.7675
H_{22}	0.7233	0.2414	0.7675	1.0000

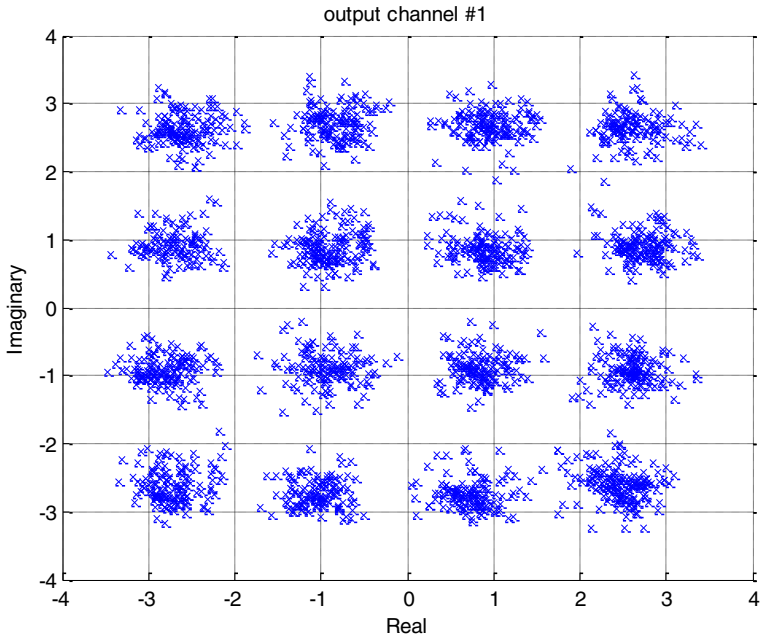

Figure 9 Output constellation; channel #1.

Discussion of the experimental results

The measurements indicate that, in a spectral bandwidth equal to 3.2 kHz, the channel gains $H_{ij}(f)$ present a low level of correlation thanks to the diversity of the two transmit polarizations and to the sensitivity of the receive antennas. In addition to the plots of the channel transfer functions which appear significantly different (Figure 8), the efficiency of the MIMO FDE equalizer (see output constellations in Figures 9 and 10) proves the non-singularity of the channel matrix which is inverted in this ZF equalizer: the four channels linking a transmitter and a receiver are not fully correlated despite absence of spatial diversity in the antenna arrays. Moreover, the measured BER underlines a good quality of service. Consequently, we can conclude that a MIMO architecture can be implemented in a trans-horizon HF

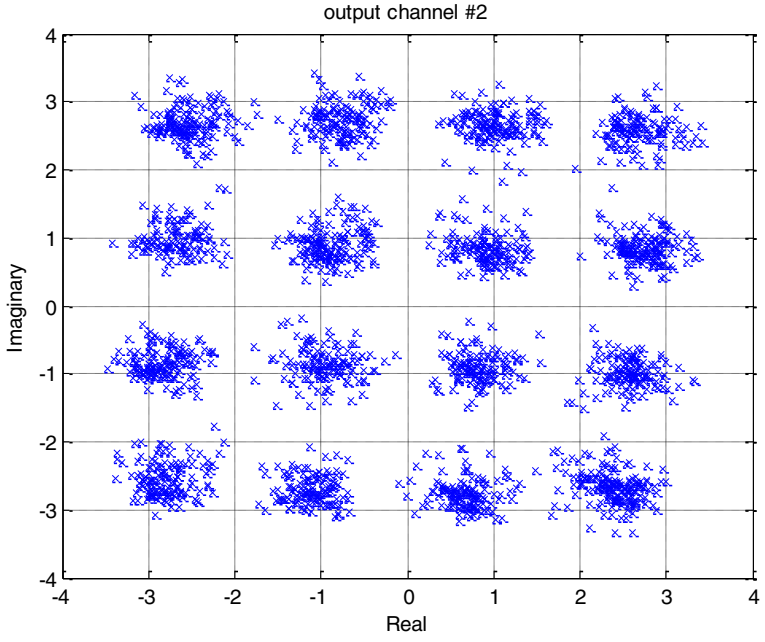

Figure 10 Output constellation; channel #2.

communication system under the condition that diverse polarizations are generated at the transmit end.

Previous characterizations of HF MIMO channels have been described by Gunashekar et al. in [17], involving different arrangements of collocated active antennas at the receive end. This receiving system takes benefit of the polarization sensitivity of the different sensors in the same way that the couple of vertical loop antennas used in our project. However, the work in [17] is based on the transmission of non-modulated carriers separated by an interval of 10 Hz to ensure their identification at the receiver; the MIMO channel is then characterized inside a narrow bandwith equal to 30 Hz. Therefore, it is not relevant to compare the channel correlation coefficients estimated in both projects as the conditions are not similar.

Conclusion

This paper presents the first realization of a trans-horizon communication system resorting to a MIMO architecture. Based on considerations of physics in the ionosphere, the original idea in this program consists in replacing the usual space diversity with diversity in the transmitted polarizations. The selected 2 × 2 MIMO solution investigates the generation of two complementary circular polarizations at the transmit end: it ultimately appears as a balanced trade-off between performance and complexity. The simulation of the global system, including a realistic model of the ionospheric channel, indicates a significant capacity gain if compared to a SISO system. An experimental validation, involving a 280-km -long radio link, confirms this prediction and underlines the possibility to reach a data rate of 24.09 kbps within a 4.2 kHz wide bandwidth with a good quality of service. This performance significantly exceeds values encountered in current standards.

Future work will investigate the implementation of a minimum mean square error frequency-domain equalizer, requesting the additional estimation of the signal-to-noise ratio, to overcome the ZF performances. Moreover, an increase in the data rate will be considered through an extension in the transmitted bandwidth.

Competing interests
The authors declare that they have no competing interests.

Author details
[1]I.E.T.R., University of Rennes, 1 Campus de Beaulieu, Rennes 35042, France.
[2]French Military Academy Saint-Cyr Coetquidan, Guer 56381, France.

Received: 12 October 2012 Accepted: 21 May 2013
Published: 17 June 2013

References

1. JA Ratcliffe, *The Magneto-ionic Theory and its Application to the Ionosphere* (Cambridge University Press, Cambridge, 1962)
2. N Abbasi, SD Gunashekar, EM Warrington, S Salous, S Feeney, L Bertel, Capacity estimation of HF-MIMO systems, in *IET International Conference IRST, April 2009* (Curran Associates, New York City, 2009), pp. 51–55
3. HJ Strangeways, Estimation of signal correlation at spaced antennas for multimoded ionospherically reflected signal and its effect on the capacity of SIMO and MIMO H.F links, in *10th IET International Conference on IRST, London, July 2006* (Curran Associates, New York City, 2006), pp. 306–310
4. K Davies, *Ionospheric radio* (Peter Peregrinus Ltd, London, 1990)
5. KG Budden, The theory of the limiting polarization of radio waves reflected from the ionosphere. Proc. Royal Soc. **215**(1121), 215–233 (1952)
6. JM Kelso, Ray tracing in the ionosphere. Radio Sci. **3**(1), 1–12 (1968)
7. PL Dyson, JA Benett, A model of the vertical distribution of the electron concentration in the ionosphere and its application to oblique propagation. Journal Atm. Terr. Physics **50**, 251–262 (1988)
8. C Brousseau, P Parion, L Bertel, Possible use of the LOCAPI ionospheric software to digital communications. Physics and Chemistry of the Earth **24**(4), 339–342 (1999)
9. RM Jones, JJ Stephenson, *A versatile three dimensional ray tracing computer program for radio waves in the ionosphere, Office of Telecommunications Report 75–76* (Washington D.C, US Government Printing Office, 1975)
10. JW Nieto, Spatial diversity and high data rate waveforms-Is it worth doing? in *IEEE MILCOM Conference*, vol. 2 (IEEE, Piscataway, , 2000), pp. 1144–1148
11. A Paulraj, R Nabar, D Gore, *Introduction to Space-Time Wireless Communications* (Cambridge University Press, Cambridge, 2003)
12. C Perrine, Y Erhel, D Lemur, A Bourdillon, Image transmission through the ionospheric channel. IEE Electronics Letters **41**(2), 80–82 (2005)
13. Y Erhel, C Perrine, C Chatellier, P Bourdon, D Lemur, High data rate radio communications through the ionospheric channel. Elsevier/International Journal on Electronics and Communications **61**(4), 270–278 (2006)
14. JP Coon, S Armour, M Beach, J McGeehan, Adaptative frequency-domain equalization for single-carrier multiple-input multiple-output transmissions. IEEE trans. on Signal Processing **53**(8), 3247–3256 (2005)
15. D Falconer, S Ariyavisitakul, A Benyamin-Seeyar, B Eidson, Frequency-domain equalization for single-carrier broadband wireless systems. IEEE Communications Magazine **40**(4), 58–66 (2002)
16. DC Chu, Polyphase codes with good periodic correlation properties. IEEE trans. Information Theory **3**(2), 531–532 (1972)
17. SD Gunashekar, EM Warrington, SM Feeney, S Salous, NM Abbasi, MIMO communications within the HF band using compact antenna arrays. Radio Sci **45**, RS6013 (2010)

doi:10.1186/1687-1499-2013-167
Cite this article as: Ndao *et al.*: Development and test of a trans-horizon communication system based on a MIMO architecture. *EURASIP Journal on Wireless Communications and Networking* 2013 **2013**:167.